Ab initio mechanism revealing for tricalcium silicate dissolution

Yunjian Li
University of Macau
Hui Pan
University of Macau https://orcid.org/0000-0002-6515-4970
Xing Ming
University of Macau
Zongjin Li (zongjinli@um.edu.mo)
University of Macau

Article

Keywords: ab initio molecular dynamics, reaction pathways, tricalcium silicate

Posted Date: November 15th, 2021

DOI: https://doi.org/10.21203/rs.3.rs-1066982/v1

Version of Record: A version of this preprint was published at Nature Communications on March 10th, 2022. See the published version at https://doi.org/10.1038/s41467-022-28932-2.

Ab initio mechanism revealing for tricalcium silicate dissolution

Yunjian Li[a], Hui Pan[a, b], Xing Ming[a], Zongjin Li[a]*

[a] Institute of Applied Physics and Materials Engineering, University of Macau, Macao SAR, 999078, P. R. China

[b] Department of Physics and Chemistry, Faculty of Science and Technology, University of Macau, Macao SAR, 999078, P. R. China

Zongjin Li: E-mail: zongjinli@um.edu.mo

Abstract

Dissolution of mineral in water is ubiquitous in nature and industry, especially for the calcium silicate species. However, the behavior of such a complex chemical reaction is still unclear at atomic level. Here, we show that the ab initio molecular dynamics and metadynamics simulations enable quantitative analyses of reaction pathways, and the thermodynamics and kinetics of calcium ion dissolution from the tricalcium silicate (Ca_3SiO_5) surface. The calcium sites with different coordination environment leads to different reaction pathways and free energy barriers. The low free energy barriers lead to that the detachment of calcium ions is a ligand exchange and auto-catalytic process. Moreover, the water adsorption, proton exchange and diffusion of water into the surface layer accelerate the leaching of calcium ions from the surface step by step. The discovery in this work thus would be a landmark for revealing the mechanism of cement hydration.

Introduction

Exploring the kinetics of dissolution and dynamic properties at the water/solid interface on the atomic scale is of great significance to understand the natural process and instruct the industrial production at macroscopic scale. This has been at the heart of numerous research fields, such as geochemistry[1, 2], drug release[3], water treatment[4] and degradation of catalysis[5]. Calcium silicate is an essential constituent in many natural minerals and has been used in a variety of fields from building materials[6, 7, 8, 9] to pharmaceutical products[3, 10]. Because of its bioactivity, biocompatibility and hydraulic nature, it is also a candidate for drug delivery[11, 12], filling and regeneration material in dentistry[13, 14] and bone tissue[15]. Above all, its application in cement is of great interest due to huge amount of usage in world widely. Tricalcium silicate (Ca_3SiO_5) is the main and most reactive calcium silicate species in ordinary Portland cement (OPC)[6]. It is well known that the cement hydration is stimulated by the dissolution of calcium ions from the Ca_3SiO_5 surfaces accompanied by the precipitation of lamellar calcium-silicate-hydrate (C-S-H), which is responsible for the cohesivity, durability and mechanical properties of concrete[16].

The Ca_3SiO_5 hydration exhibits clear stages (initial, induction, acceleration and deceleration) and is governed by multiple coupled parameters diverging in different time scales (from fs to years) and space scales (from nanoscale to macroscale), which is extremely complex to depict precisely. The experimental studies found that during the dissolution process the surface topography undergoes a complicated transformation with the formation of etch pits, point defects and screw dislocation[17]. Besides, the hydrated silicate species above the surfaces reconstruct with the remaining Ca ions after the detachment of Ca ions[18, 19]. In general, the dissolution rate is well accepted to be affected by the grain particles size, overall reactive surface area, temperature, components of solution and dislocations on the solid surface[20] on the macroscopic scale. Alongside these, the global dissolution rate is also controlled by the slowest step, which depends on the individual stage during reaction. However, the case would

be more intricate for Ca_3SiO_5 due to the coupling effect with the precipitation of hydrate product. It has been observed the dissolution rate of Ca_3SiO_5 is extremely fast initially and then decreases dramatically from the highest to the lowest[21]. The reasons for this phenomenon are still on debate. Firstly, the hydroxylation prior to dissolution may stabilize the surface and therefore lower the solubility of Ca_3SiO_5, as is the case for other minerals[20]. Furthermore, the dissolution theory[17] implies the driving force for the initial swift dissolution rate is the high degrees of undersaturation as it is energetically favorable for etch pits to form. When the composition of the solution is very close to the solubility equilibrium of Ca_3SiO_5, the etch pits no longer form and even step retreat, thus limiting the dissolution rate rather severely[22], like the natural weathering[23] and other mineral hydration[23]. Moreover, there may also be an electrical double layer[24] and a metastable hydrate phase barrier[21] formed on the Ca_3SiO_5 surface. All these hypotheses and the fit of the calorimetric curve of Ca_3SiO_5 hydration using thermodynamic calculations[25] may be derived from the ignorance on the interfacial reactions during the Ca_3SiO_5 dissolution, especially the dissolution behavior of calcium ions at atomic level.

Fortunately, atomistic simulations can tackle these problems. The previous density functional theory (DFT) -based geometry optimization calculations[26] indicated the adsorption of water on the Ca ion impairs the bonds strength between the calcium and oxygen ions on the surface. Claverie et al.[27] investigated the proton transfer at the water/Ca_3SiO_5 interface using ab initio molecular dynamics (AIMD) simulations and found that the hydroxides formed on the surface are highly stable. However, they did not observe an obvious vertical displacement of Ca ions relative to the initial position. In fact, it is very hard to probe a complete calcium dissolution process at the atomic level even using the traditional molecular dynamics (MD) simulations[28, 29] with large timescale (i.e. nanoseconds). Moreover, the classical MD is not appropriate to simulate the chemical reaction involving the breakage and formation of bonds.

Even using the ReaxFF force field is still not preciously enough to present the reaction pathways for a chemical reaction. Hence, it is indispensable to give an ab initio description of such a fundamental reaction.

Here, we uncover, for the first time, the dissolution mechanism of Ca_3SiO_5 at early stage with ab initio method. We calculated the reaction pathways, free energy changes and free energy barriers of Ca_3SiO_5 dissolution using the ab initio metadynamics simulations. We show that the calcium dissolution at different sites have different reaction pathways and the less coordinated Ca is easier to escape from the surface. Besides, we found that water molecules can reduce the dissolution free energy barriers not only by attractive effect through adsorbing on Ca, but also by repulsive effect through proton penetrating into the surface and water diffusion to the original Ca site. Our findings pave the way to the atomistic understanding of surface reaction for the Ca dissolution from Ca_3SiO_5.

Results

Dissolution pathways for Ca_α. The chemical reaction in initial Ca_3SiO_5 hydration, especially the dissolution of Ca ions, is a process of breaking the old Ca-O_s bonds and forming new Ca-O_w bonds. Therefore, we probe into the coordination environment of Ca to calculate the full dissolution pathways. There are four Ca sites in different chemical environment on the Ca_3SiO_5 (111) surface and generally they can be classified into three- and five- coordinated Ca species, which are indicated by Ca_α and Ca_β in this work, respectively. The Ca_3SiO_5 dissolution rate at different surface site (i.e. flat, step and kink site) is typically different due to different coordination environments around Ca, which changes the dissolution pathways as well as the thermodynamic and kinetic properties. Thus, we would investigate the dissolution mechanism for both Ca_α and Ca_β.

For the dissolution of Ca_α, we can clearly identify six free energy minima on the two-

dimensional (2D) free energy surface (FES) (Figure 1b). In addition, the free energy basins and free energy barriers along any one of collective variables (CVs) can also be found through the one-dimensional (1D) FES projected from the 2D FES (Figures 1a and c). When the water encounters with the Ca_3SiO_5 surface, the stable state changes from (3, 0) (the state before water contacting the substrate) to A(3, 2), indicating two water molecules adsorb on Ca_α and make the system more stable. After crossing two energy barriers ($\Delta A^{\ddagger}$(A-B) = 3.57 kJ/mol and $\Delta A^{\ddagger}$(B-C)) = 11.76 kJ/mol), the system comes to the most stable state C(3, 4) with up to four adsorbed water molecules. This high-coordination (seven-coordinated) state compromises the breakage of the original Ca-O_s bond but associated with huge free energy barriers ($\Delta A^{\ddagger}$(C-D)) = 15.71 kJ/mol and $\Delta A^{\ddagger}$(D-E)) = 14.28 kJ/mol) and a little increase in free energy changes (ΔA(C-D = 4.69 kJ/mol and ΔA(D-E) = 3.48 kJ/mol)) . The breakage of the Ca-O bond with the oxygen ion from silicate is earlier, but more difficult than that with the interstitial oxygen ion (from the state C to D to E). These two sequential steps of breaking Ca-O_s bonds decrease the total coordination number from seven to five, making this detached and free Ca ion have more chances to accommodate one more water ligand and reform an octahedral structure, albeit at this stage is severely distorted with a trigonal bipyramid (D_{3h}) structure. The free energy barrier and the free energy change for these steps ($\Delta A^{\ddagger}$(E-F) = 8.70 kJ/mol and ΔA(E-F) = -3.87 kJ/mol) are relatively high compared to the same fivefold to sixfold coordination transition step (A-B).

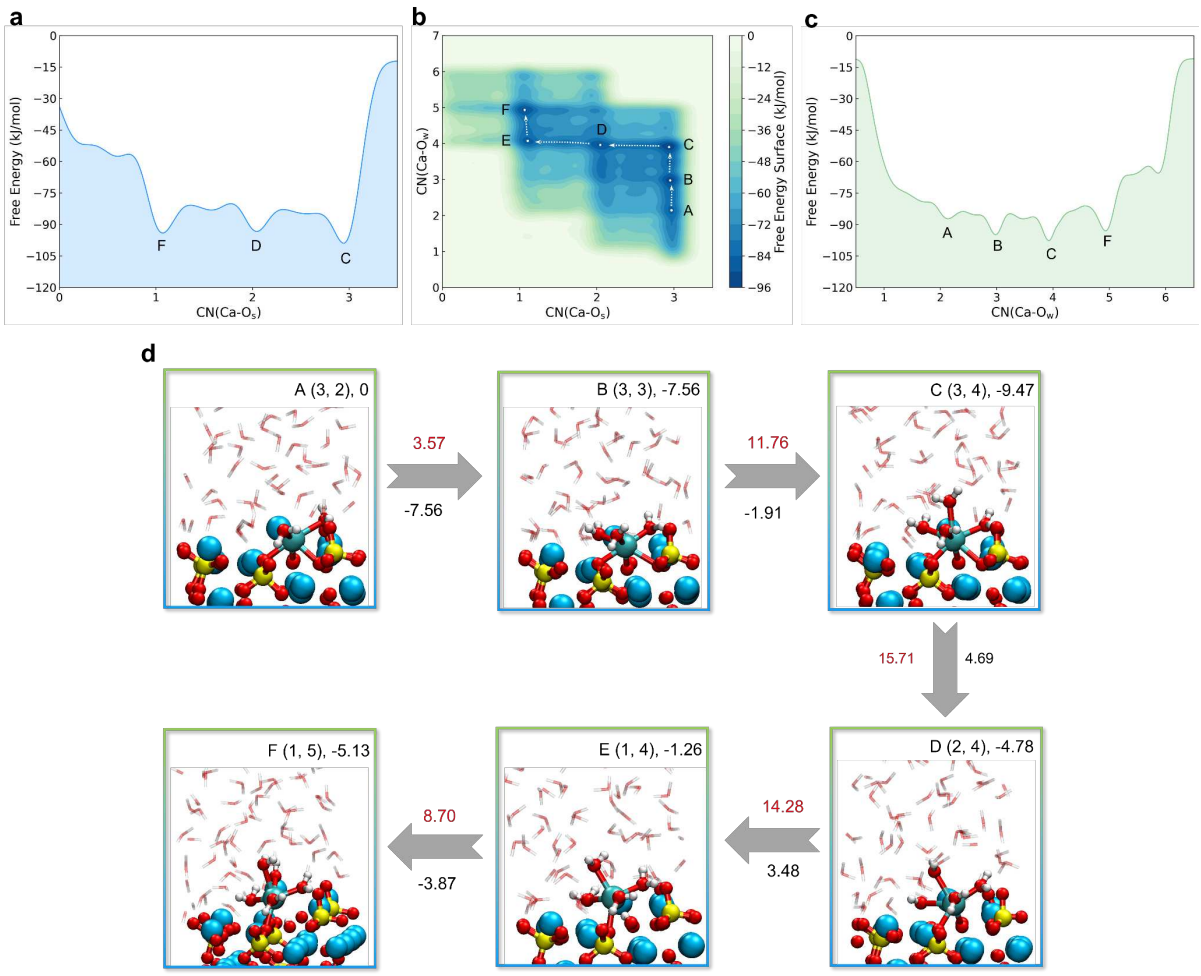

Figure 1. Dissolution mechanism of Ca_{α} from the Ca_3SiO_5 surface. **a, c** The one-dimensional free energy profiles with respect to CN(Ca-O_s) and CN(Ca-O_w), respectively. **b** The two-dimensional free energy surface with variables of CN(Ca-O_s) and CN(Ca-O_w). **d** The configurations of the free energy minimum states on the FES and the corresponding reaction pathways. The state number, coordinates on the FES and the Helmholtz free energy values (kJ/mol) relative to state A are at the upper right. The values (kJ/mol) in red are free energy barriers and the values under the arrows in black are overall changes in free energies between two states. The yellow, blue, cyan, red and white spheres are indicted to the silicon, calcium (no bias potential), calcium (with bias potential), oxygen and hydrogen ions, respectively. For simplicity, the solute is shown in the transparent stick type.

Dissolution pathways for Ca_β with CN(Ca-O_s) from 5 to 2. The surface reactivity varies with the different sites on the Ca_3SiO_5 surface and the hydration process is closely correlated with the coordination number of surface Ca ions[29]. Thus, we carried out the comparative WT-MetaD simulations for Ca_β to investigate whether the dissolution pathway alters with initial coordination environment. Obviously, the FES for the detachment of Ca_β is different from that for Ca_α (Figures 2a, b and c) and becomes more complicated with more possible reaction pathways. When water molecules come to the Ca_3SiO_5 surface, the first stable state is A(5, 1). Albeit the number of water molecule is less than that for Ca_α, the total coordination number is same with six. However, the reaction pathway for the next step is more complex. The state A has two potential reaction paths to adsorb more water molecules. The first one adsorbs one more water molecule directly without breaking the Ca-O_s bond (A-B). While the other one does it by breaking two Ca-O_s bonds at the same time (A-D). From a thermodynamic point of view, it is more energetically favourable to pass through state B first due to the larger free energy change between the state A and the second free energy minimum. Nevertheless, from a kinetic point of view, it is rapider to react along the pathway of A-D because of its lower free energy barriers ($\Delta A^{\ddagger}$(A-D) = 6.49 kJ/mol and $\Delta A^{\ddagger}$(A-B) = 7.01 kJ/mol). The reaction pathway of A-B-C-D is similar to the B-C-D-E for the dissolution of Ca_α, in which the start of Ca-O_s bond cleavage is from the sevenfold coordination state. Noticeably, the seven-coordinated species is an essential intermediate in the dissolution of Ca, which is similar to the decomposition of γ-Al_2O_3[30]. But the free energy barriers along the B-C-D ($\Delta A^{\ddagger}$(B-C) = 7.38 kJ/mol, $\Delta A^{\ddagger}$(C-D) = 4.24 kJ/mol) is much smaller than that along C-D-E for Ca_α. The state D(3, 2) is the most stable state with the same coordinate of the start point, A, on the FES of Ca_α and is also a new outset for other two different reaction pathways towards breaking one more Ca-O_s bond. The reaction would be more possible to proceed in the direction from D to E(2, 2) due to the lower free energy barrier ($\Delta A^{\ddagger}$(D-E) = 19.60 kJ/mol) compared to the route from D to G(2, 3) ($\Delta A^{\ddagger}$(D-E)

= 29.02 kJ/mol, $\Delta A^{\ddagger}$(E-F)=26.11 kJ/mol)) and it is the rate-controlling step among all the reactions. It should be noted that the further Ca-O_s bond cleavage from 2 to 0 is not accessible during this simulation due to the large free energy barriers required. Therefore, to uncover the subsequent dissolution mechanism of Ca with less than two- and even zero-coordinated O_s, it is necessary to add a 'wall' to constrain the CVs in the region of interest.

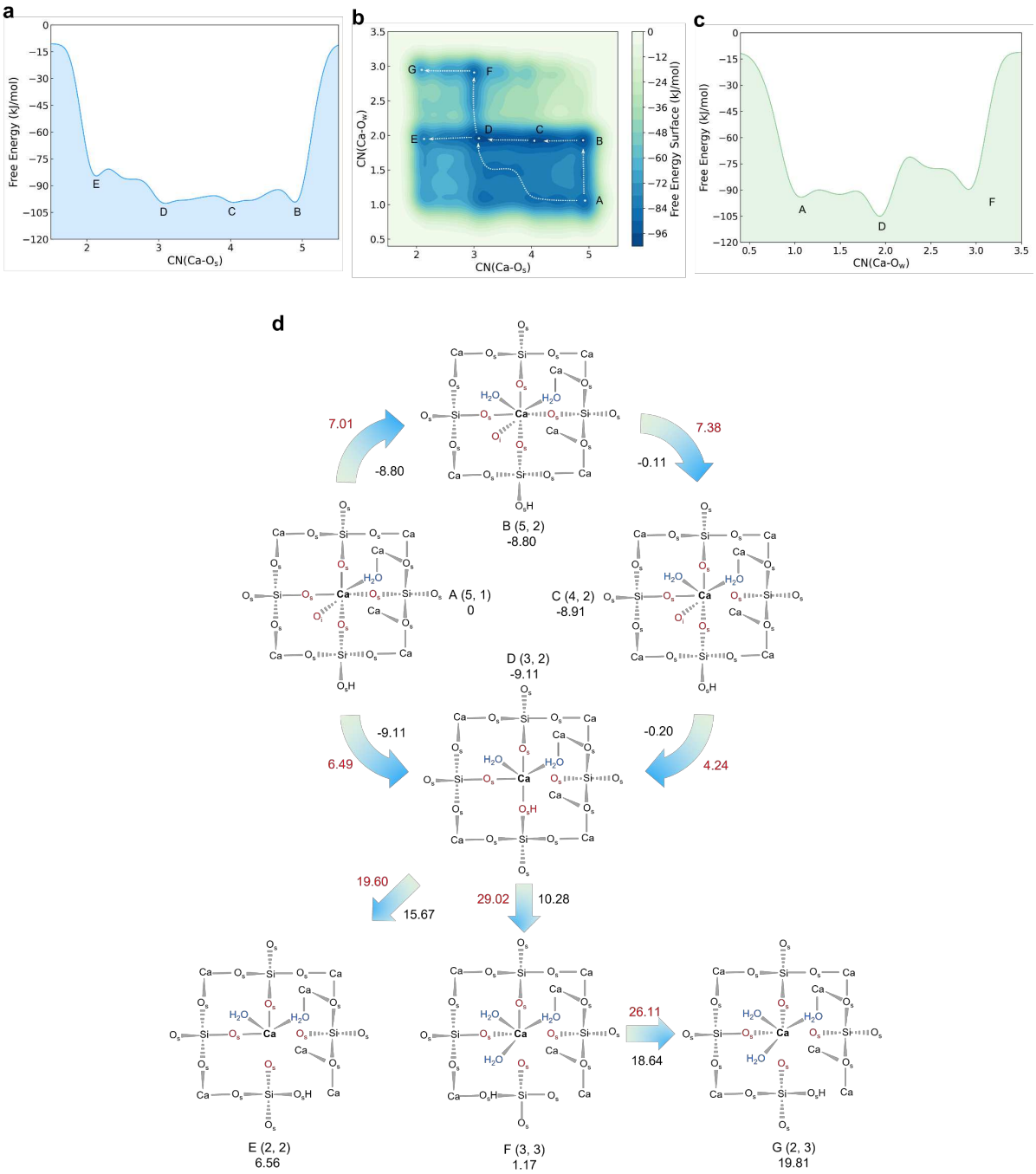

Figure 2. Dissolution mechanism of Caβ from the Ca_3SiO_5 surface with CN(Ca-O_s) from 5 to

2. **a, c** The one-dimensional free energy profiles with respect to CN(Ca-O_s) and CN(Ca-O_w), respectively. **b** The two-dimensional free energy surface with variables of CN(Ca-O_s) and CN(Ca-O_w). **d** The overhead sketches for the first layer of the Ca_3SiO_5 surface of the free energy minimum states on the FES (the all-atom configurations is presented in Supplementary Figure 1) and the corresponding reaction pathways. The state number, coordinates on the FES and the Helmholtz free energy values (kJ/mol) relative to state A are presented around the corresponding structure. The values (kJ/mol) in red are free energy barriers and the values under the arrows in black are overall changes in free energies between two states. The biased Ca_β is bolded, and the O_s and O_w bonded with Ca_β were highlighted in red and blue, respectively.

Complete dissolution of Ca_β with CN(Ca-O_s) from 2 to 0. For the further detachment of Ca_β with CN(Ca-O_s) from 2 to 0, we assume that the start point is the most stable state H(1, 4) on the FES (Figure 3a) as it is most possible to exist in reality. To further dissolve, Ca_β needs to guest a water molecule first to achieve an octahedral structure crossing over a 26.99kJ/mol free energy barrier and coming to the state I(1, 5) (Figure 3b). The next step of welcoming one more water molecule from the state I to K(1, 6) is the rate-controlling step due to the highest free energy barrier of 28.08 kJ/mol. After that, Ca_β detaches from the original position progressively and finally gets rid of the confinement of O_s network totally, which is hydrated by the surrounding water molecules to the six- or seven-coordinated solute ion. The five-, six- and seven-coordinated Ca_β ion can be transformed to each other. However, the sixfold coordination state processes the greatest possibility, not only because the reactions from the fivefold state M(0, 5) and sevenfold state L(0, 7) to the sixfold state K(0, 6) are spontaneous (ΔA(M-K) = -2.09 kJ/mol and ΔA(L-K) = -10.30 kJ/mol), but also the free energy barriers ($\Delta A^{\ddagger}$(M-K)=10.34 kJ/mol, $\Delta A^{\ddagger}$(L-K)=6.96 kJ/mol) are lower than those of the reverse reactions, which is confirmed by a further 30 ps equilibrium AIMD simulations. The AIMD also show that the

coordinated O_w with Ca_β increased slightly and the dissolved Ca forms a more regular octahedral structure with water and hydroxyl with the evolution of time.

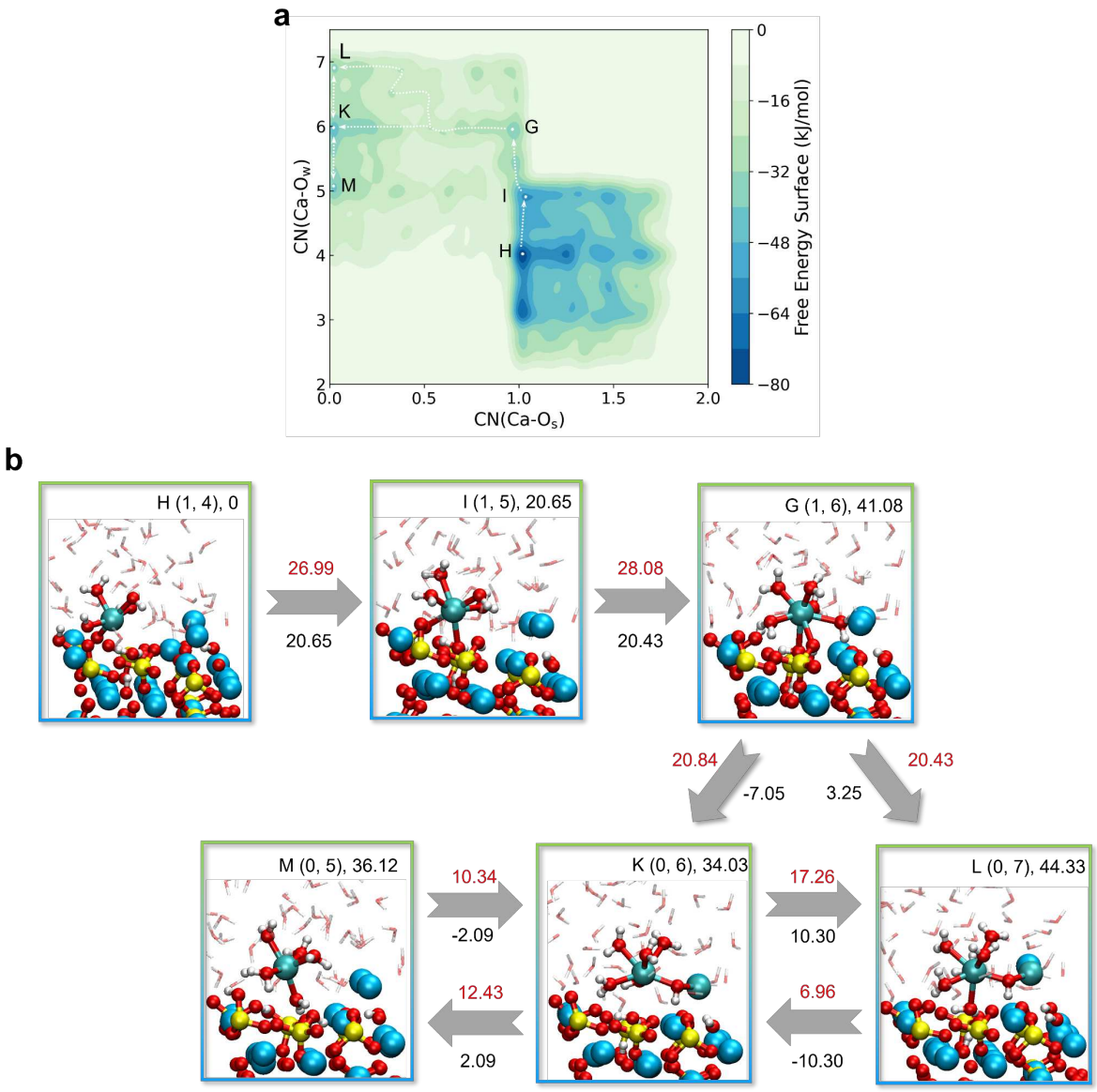

Figure 3. The further dissolution mechanism of Ca_β from the Ca_3SiO_5 surface with CN(Ca-O_s) from 2 to 0. **a** The two-dimensional free energy surface with variables of CN(Ca-O_s) and CN(Ca-O_w). **b** The configurations of the free energy minimum states on the FES and the corresponding reaction pathways. The state number, coordinates on the FES and the Helmholtz free energy values (kJ/mol) relative to state H are at the upper right. The values (kJ/mol) in red

are free energy barriers and the values under the arrows in black are overall changes in free energies between two states.

Structural and dynamic analysis of the water/Ca_3SiO_5 interface after the dissolution of the Ca ion. According to the atomic density and atomic excess profiles (Figure 4a), we define six regions for the water structure along the z direction on the Ca_3SiO_5 surface. It is obvious that the H ion penetrates into the second layer of the surface (z = 6 Å) due to the escape of the Ca ion and the proton exchange, which is the first time for such a phenomenon in the hydration of Ca_3SiO_5 to be observed by the AIMD simulation. The region II is the chemisorbed water molecule and III is a mixture of the physisorbed water molecule for the surface and the first hydration shell of the dissolved Ca, which expands the destruction area of the layered water structure compared to the surface before dissolution. The region IV, V and VI are the transition layer, bulk layer and water/vacuum layer, respectively, which are similar to those on the perfect Ca_3SiO_5 surface. The radial distribution function (RDF) (Figure 3b) shows that the first and second hydration shells of the dissolved Ca are more than that of the surface Ca. It also presents that the Ca-O_w bond length for the dissolved Ca is 2.39 Å, which is shorter than that for surface Ca with 2.50 Å, indicating a stronger interaction between Ca and the water molecule after dissolving. The mean square displacement (MSD) (Figure 3c) presents a more dynamic property and stronger diffusion ability for the dissolved Ca compared to the previous surface state. We also calculated the infrared (IR) spectra for the system and extract the parts for Si-OH and Ca-OH. It clearly shows one band at 916 cm^{-1} (Figure 4d), which is characteristic for the Si-OH bond raised in experimental IR spectra upon Ca_3SiO_5 hydration[19]. In addition, two bands arising at 700-1000cm^{-1} and 3640 cm^{-1} (Figure 4e) shows the formation of Ca-OH during the dissolution of Ca ion as indicated by the experimental results[19, 31]. From the transmission electron microscopy (TEM) photograph (figure 4f), we can clear see when Ca_3SiO_5 encounters

with water, the Ca cations are released from the Ca_3SiO_5 surface and form the $Ca(OH)_2$ in the aqueous solution. An atomistic interpretation of this natural phenomenon can be obtained from our AIMD simulation, which shows the Ca ion coordinated with five water molecules and one hydroxyl group releases from the Ca_3SiO_5 surface following the proton transfer from the water molecule to the second layer of the interstitial oxygen ion and the occupation of the initial Ca site by one water molecule. This water molecule is parallel to the surface and form hydrogen bond with the new formed O-H and O_s.

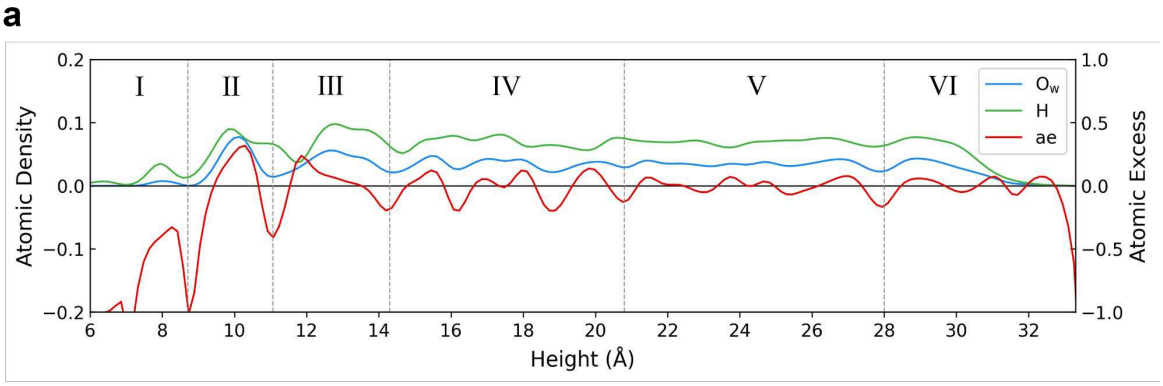
a
I
II
III
IV
V
VI
O_w
H
ae
Atomic Density
Atomic Excess
Height (Å)

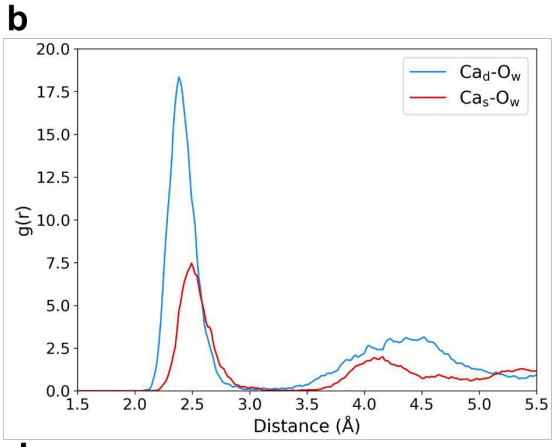
b
Ca_d-O_w
Ca_s-O_w
g(r)
Distance (Å)

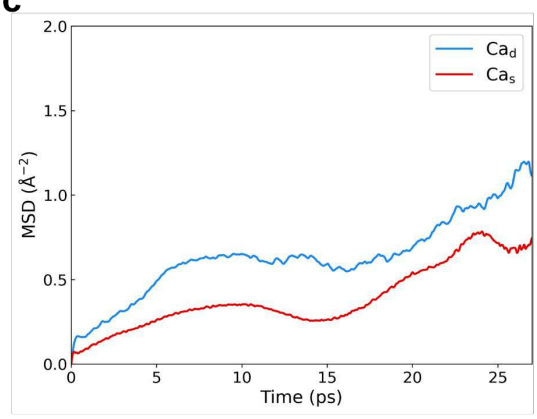
c
Ca_d
Ca_s
MSD (Å^{-2})
Time (ps)

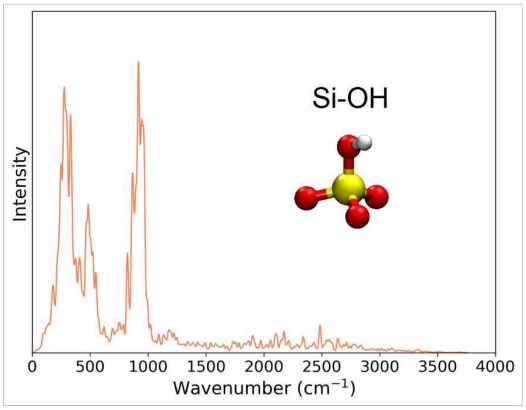
d
Si-OH
Intensity
Wavenumber (cm^{-1})

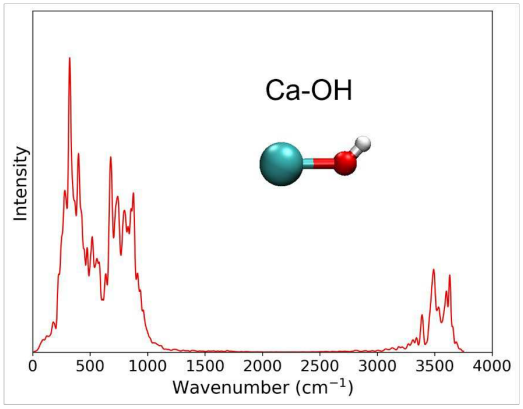
e
Ca-OH
Intensity
Wavenumber (cm^{-1})

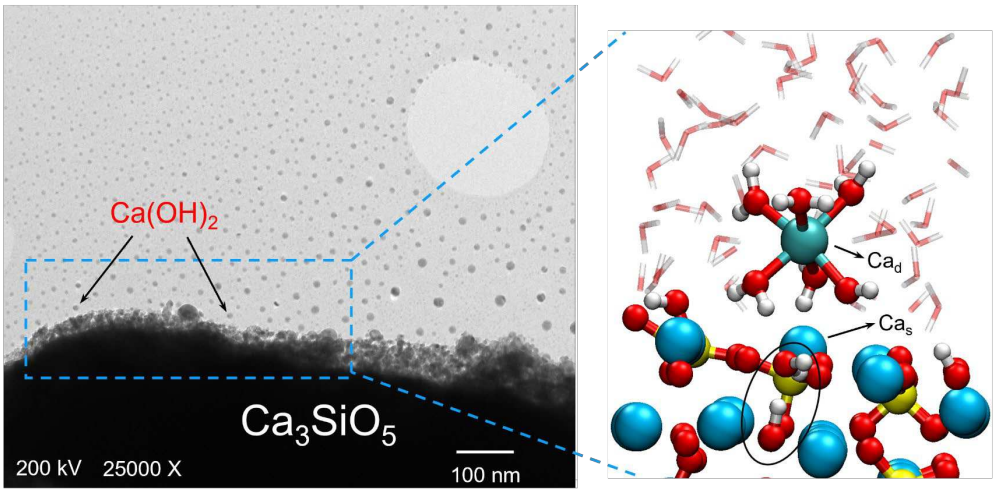
f
$Ca(OH)_2$
Ca_3SiO_5
200 kV 25000 X
100 nm
Ca_d
Ca_s

Figure 4. **a** Atomic density for O_w and H, and atomic excess profiles as a function of the height beginning at 6 Å from the bottom of the Ca_3SiO_5 surface. **b** Radial distribution function (RDF) between the dissolved Ca ion (Ca_d) and O_w as well as between the surface Ca ion in the same site (Ca_s) and O_w. **c** The mean square displacement (MSD) evolution of Ca_d and Ca_s. **d, e** IR spectrums for Si-OH group and Ca-OH group, respectively. **f** TEM image of the dissolution of Ca from the Ca_3SiO_5 surface and the snapshot of the equilibrium AIMD at 30 ps. The composition and the electron diffraction patterns of $Ca(OH)_2$ refers to [32]

Discussion

The calcium sites with different coordination environments lead to different reaction pathways and free energy barriers. The dissolution of three-coordinated Ca_α is easier than the five-coordinated Ca_β not only because of its initial less restraint from the Ca_3SiO_5 surface, but also the smaller free energy barriers along the reaction path. In addition, The free energy barriers between the two stable states on either FES of Ca_α and Ca_β tends to be larger as the Ca-O_s bonds become less, which means the water adsorption on the Ca_3SiO_5 surface is easier than the detachment of Ca and the kinetic rate decreases gradually as this process proceeds. Nonetheless even the highest free energy barrier is only 29.02 kJ/mol, which is easy to be crossed, suggesting the dissolution is an auto-catalytic process. It should be noted that there is no human intervention during the simulation of crossing over the free energy barriers, which ensures the reliability of our results. Thus, the results obtained in this work are general and applicable to other kinds of calcium silicate species.

Our ab initio WT-MetaD simulations with explicit water solvation highlight the importance of the water molecule on the detachment of Ca during the Ca_3SiO_5 hydration. In short, the dissolution of Ca can be explained in terms of a ligand exchange process. It initially stimulated by the water adsorption, raising the total coordination number with oxygen ions to

a high level (five to seven). The adsorbed water molecules can reduce the free energy barriers for breaking the Ca-O_s bond, and thus provide an opportunity for Ca to break the Ca-O_s bonds with the optimal six coordination number unchanged. In fact, the breakage of Ca-O_s bonds is a multi-step and multi-orientation chemical reaction, and every step needs a relatively high free energy barrier, which is strait to cross for traditional AIMD simulations within 100 ps but easy in reality. In addition, the dissolution of Ca is further promoted by the proton exchange and the diffusion of water molecule from the chemisorbed layer into the second surface layer. On the one hand, the H ion penetrate into the second layer of the surface and bonds to the interstitial oxygen ion previously bonded to the dissolved Ca ion, leading to a repulsive force pushing Ca out of the surface. At the same time, this diffused water molecule resides in the position of the Ca ion before dissolution and forms the hydron bond network with O_s, O_w and H, which undermines the attractive force to this Ca.

In summary, an atomistic and mechanistic picture of Ca dissolution from the Ca_3SiO_5 surface in water solution at the initial stage of Ca_3SiO_5 hydration is investigated using the ab initio molecular dynamics and metadynamics simulations. We find that the Ca dissolution from the Ca_3SiO_5 are multi-step and multi-orientation chemical reactions accompanied by the water adsorption, proton exchange, breakage of Ca-O_s bonds and water diffusion. The thermodynamic and kinetic analyses show that the detachment of Ca is spontaneous when the Ca is not fully dissolved and unspontaneous when Ca is no more coordinated with O_s. Additionally, the Ca dissolution is an auto-catalytic process with the highest free energy barriers of only 29 kJ/mol. The reaction pathways for Ca in different coordination environments are different and the less coordinated Ca is easier to leach from the surface. Besides, we find the water molecules provide not only the attractive forces pulling Ca out of the surface, but also repulsive forces in filling the precious Ca site and pushing it away. The present achievement thus provides an insight into the cement hydration and also predict the evolution

of other complex geochemical and catalytic systems.

Methods

Atomistic model

The Ca_3SiO_5 (111) surface was cleaved from the M3 type of Ca_3SiO_5 (obtained from CCSD[33]), which is most frequently observed in industrial clinkers[34]. The details of the DFT-based geometry optimization of the bulk crystal and surface slab were listed in Supplementary Methods. Considering the adsorption of water molecule on the Ca_3SiO_5 surface occurs even before contacting bulk water[35], we firstly adsorbed isolated water molecules to saturate the dangling bond on the Ca_3SiO_5 surface. Then, we put a 20 Å thick layer of water with density of 1g/cm^3 on the Ca_3SiO_5 (111) surface (totally 333 atoms) for the dissolution simulations. The lattice parameters were 14.21 Å × 11.72 Å × 36 Å after setting a vacuum of 15 Å along z direction. After the detachment of the Ca_β ion from its initial position to the state of D, we further constructed a new model (14.21 Å × 11.72 Å × 48 Å) by adding another 10 Å thick layer of water on the previous system (totally 498 atoms) to calculate the structural and dynamic properties of the equilibrium state.

AIMD simulations

All the AIMD simulations reported in this work were performed within the framework of DFT with the generalized gradient approximation (GGA) using the Perdew-Burke-Ernzerhof (PBE)[36] functional and Grimme D3 correction[37], which was implemented in the CP2K/Quickstep[38]. The Core electrons were described by Goedecker-Teter-Hutter (GTH) pseudopotentials[39, 40] and the valence electrons were described by a mixed Gaussian and plane waves basis (GPW)[41]. The wave functions were expanded on a double-ζ valence polarized

(DZVP) basis set along with an auxiliary plane wave basis set at a cutoff energy of 500 Ry. The Brillouin zone was sampled by the gamma approximation. During AIMD, the nuclei were treated within the Born–Oppenheimer approximation with a timestep of 0.5 fs for equilibrium simulation, while 1 fs for metadynamics simulations with the replacement of hydrogen by deuterium to accelerate the structural evolution without energy drifts[27, 42]. The temperature was maintained at 300 K using a Nosé-Hoover thermostat[43, 44] coupled to the system with a time constant of 1000 fs in the Canonical ensemble (NVT). The convergence criterion for energy was set to 10^{-12} Hartree and for self-consistent field was 10^{-6} Hartree. All the system were first optimized to a stable state and then thermalized for at least 2.5 ps before the production run for statistical analysis. The duration of the AIMD simulations for dissolution of Ca_{α}, dissolution of Ca_{β} with CN(Ca-O_s) from 5 to 2, further dissolution of Ca_{β} with CN (Ca-O_s) from 2 to 0, equilibrium of final state of Ca_{β} were 100 ps, 63 ps, 46ps, and 30ps, respectively.

Metadynamics simulations

In the well-tempered ab initio metadynamics[45] (WT-MetaD) simulations, we utilized a two-dimensional collective variables (CVs) characterized by the coordination number (CN) to monitor the dissolution process. The CN(Ca-O_s) is the coordination number of the Ca ion with all oxygen ions from the surface slab, while CN(Ca-O_w) is the coordination number of the Ca ion with all oxygen ions from water molecules. As defined in the PLUMED code[46], the CN have the expression as follows:

$$CN\left(Ca, O_{w/s}\right) = \sum_{j \in O_{w/s}} s_{ij}\left(r_{ij}\right) = \sum_{j \in O_{w/s}} \frac{1 - \left(\frac{r_{ij} - d_0}{r_0}\right)^n}{1 - \left(\frac{r_{ij} - d_0}{r_0}\right)^m} \quad (1)$$

where r_{ij} is the distance between atom i and atom j. s_{ij} (r_{ij}) is a rational type of switching function describing the coordination between atom i and j. d_0 is the central value of the function. r_0 is the acceptance distance of the switching function, where the function well be n/m at d_0+ r_0.

Here, we define d_0 is 2.42 Å, which is the equilibrium bond length between the Ca and O ions[47]; r_0 is 0.4 Å, which is around half of the full width at half maximum of the radial distribution function of Ca-O[48] and n and m are 6 and 12, respectively.

The Gaussian hills was deposited every 30 timesteps with the initial height of 3.5 kJ/mol and width of 0.15 for both CVs. The biasfactor were 15 for simulations of Ca_α and 24 for simulation of Ca_β. In addition, to further investigation of the dissolution process to a larger extent, we added a quadratic wall with the force constant of 500 kJ/mol at the position of CN(Ca-O_s) equals to 1.5 to restrict the simulation of further dissolution of Ca_β on the regions of free energy surface with CN(Ca-O_s) less than 1.5. The time evolutions of the CV1 and CV2, the convergence tests for the free energy surfaces and the errors between the free energy minima were shown in Supplementary Figures 2-7.

Structural and spectroscopy calculations

The atomic excess (ae) is defined as:

$$ae = \frac{2[Ow] - 2[H]}{2[Ow] + 2[H]} \tag{2}$$

where $[Ow]$ and $[H]$ are atomic density for Ow and H, respectively. The negative value for ae indicates an excess of Ow, while the positive one indicates an excess of H.

For the vibrational spectra, we use the last 30 ps equilibrium AIMD trajectory to calculate the infrared (IR) spectrum with the TRAVIS program[46]. The molecular electric properties were calculated every 4 fs (8 timesteps) using the Voronoi integration approach[49]. The IR spectrum of particular components of a system were computed though the Fourier transform of the molecular dipole autocorrelation function as follows:

$$A(\omega) \propto \int \langle \dot{\mu}(\tau)\dot{\mu}(t+\tau)\rangle_\tau e^{-i\omega t} dt \tag{3}$$

where A is the absorption cross section, ω is frequency, and $\dot{\mu}$ is the time derivative of the

dipole moment leading to the dipole-velocity autocorrelation function.

Synthesis of Ca_3SiO_5 and characterization of dissolution of Ca_3SiO_5

The synthesis of Ca_3SiO_5 was conducted through a traditional method[50]. Calcium carbonate and silica with molar ratio of 3:1 was first ground to pass through a 63-μm sieve and then evenly mixed for 2 h. The obtained fine powder was compressed into pancakes in a lab press and put into a Pt crucible for calcination at 1500 °C for 5 h, and quickly cooled down to ambient temperature within 10 min. The obtained product was ground into fine powder, compressed and recalcined for four repeating cycles before the production of pure Ca_3SiO_5. The synthetic Ca_3SiO_5 was then dispersed in the water solution for hydrolysis.

The morphology of dissolution of Ca_3SiO_5 was characterized by transmission electron microscopy (JEOL, JEM-2100, 200 kV), equipped with an energy dispersive spectroscopy system.

References

1. Schliemann R, Churakov SV. Atomic scale mechanism of clay minerals dissolution revealed by ab initio simulations. *Geochimica et Cosmochimica Acta* 2021, **293:** 438-460.

2. Ye S, Feng P, Liu Y, Liu J, Bullard JW. In situ nano-scale observation of C3A dissolution in water. *Cement and Concrete Research* 2020, **132:** 106044.

3. Sato H, Miyagawa Y, Okabe T, Miyajima M, Sunada H. Dissolution mechanism of diclofenac sodium from wax matrix granules. *Journal of pharmaceutical sciences* 1997, **86**(8)**:** 929-934.

4. Pirkanniemi K, Sillanpää M. Heterogeneous water phase catalysis as an environmental application: a review. *Chemosphere* 2002, **48**(10)**:** 1047-1060.

5. Ravenelle RM, Copeland JR, Kim W-G, Crittenden JC, Sievers C. Structural changes of γ-Al2O3-supported catalysts in hot liquid water. *Acs Catalysis* 2011, **1**(5)**:** 552-561.

6. Taylor HF. *Cement chemistry*, vol. 2. Thomas Telford London, 1997.

7. Vogel W. *Glass chemistry*. Springer Science & Business Media, 2012.

8. Rodrıguez J, Rodrıguez M, De Aza S, Pena P. Reaction sintering of zircon–dolomite mixtures. *Journal of the European Ceramic Society* 2001, **21**(3)**:** 343-354.

9. Zheng Q, Wang W. Calcium silicate based high efficiency thermal insulation. *British ceramic transactions* 2000, **99**(4)**:** 187-190.

10. Kinoshita M, Baba K, Nagayasu A, Yamabe K, Shimooka T, Takeichi Yi*, et al.* Improvement of solubility and oral bioavailability of a poorly water-soluble drug, TAS-301, by its melt-adsorption on a porous calcium silicate. *Journal of pharmaceutical sciences* 2002, **91**(2)**:** 362-370.

11. Zhu Y-J, Guo X-X, Sham T-K. Calcium silicate-based drug delivery systems. *Expert opinion on drug delivery* 2017, **14**(2)**:** 215-228.

12. Jain SK, Awasthi A, Jain N, Agrawal G. Calcium silicate based microspheres of repaglinide for gastroretentive floating drug delivery: Preparation and in vitro characterization. *Journal of controlled release* 2005, **107**(2)**:** 300-309.

13. Prati C, Gandolfi MG. Calcium silicate bioactive cements: Biological perspectives and clinical applications. *Dental materials* 2015, **31**(4)**:** 351-370.

14. Xu S, Lin K, Wang Z, Chang J, Wang L, Lu J*, et al.* Reconstruction of calvarial defect of rabbits using porous calcium silicate bioactive ceramics. *Biomaterials* 2008, **29**(17)**:** 2588-2596.

15. Ding S-J, Shie M-Y, Wang C-Y. Novel fast-setting calcium silicate bone cements with high bioactivity and enhanced osteogenesis in vitro. *Journal of Materials Chemistry* 2009, **19**(8)**:** 1183-1190.

16. Zongjin L. Advanced concrete technology. *Hoboken, New Jersey: John Wiley & Sons, Inc* 2011.

17. Juilland P, Gallucci E, Flatt R, Scrivener K. Dissolution theory applied to the induction period in alite hydration. *Cement and Concrete Research* 2010, **40**(6)**:** 831-844.

18. Pustovgar E, Sangodkar RP, Andreev AS, Palacios M, Chmelka BF, Flatt RJ*, et al.* Understanding silicate hydration from quantitative analyses of hydrating tricalcium silicates. *Nature communications* 2016, **7**(1)**:** 1-9.

19. Higl J, Hinder D, Rathgeber C, Ramming B, Lindén M. Detailed in situ ATR-FTIR spectroscopy study of the early stages of CSH formation during hydration of monoclinic C3S. *Cement and Concrete Research* 2021, **142:** 106367.

20. Bellmann F, Sowoidnich T, Ludwig H-M, Damidot D. Dissolution rates during the early hydration of tricalcium silicate. *Cement and Concrete Research* 2015, **72:** 108-116.

21. Naber C, Bellmann F, Neubauer J. Influence of w/s ratio on alite dissolution and CSH precipitation rates during hydration. *Cement and Concrete Research* 2020, **134:** 106087.

22. Nicoleau L, Bertolim MA. Analytical model for the alite (C3S) dissolution topography. *Journal of the American Ceramic Society* 2016, **99**(3)**:** 773-786.

23. Lasaga AC, Luttge A. Variation of crystal dissolution rate based on a dissolution stepwave model. *Science* 2001, **291**(5512)**:** 2400-2404.

24. Tadros M, Skalny J, Kalyoncu R. Early hydration of tricalcium silicate. *Journal of the American Ceramic Society* 1976, **59**(7-8)**:** 344-347.

25. Zhang Z, Han F, Yan P. Modelling the dissolution and precipitation process of the early hydration of C3S. *Cement and Concrete Research* 2020, **136:** 106174.

26. Qi C, Spagnoli D, Fourie A. DFT-D study of single water adsorption on low-index surfaces of calcium silicate phases in cement. *Applied Surface Science* 2020, **518:** 146255.

27. Claverie J, Bernard F, Cordeiro JMM, Kamali-Bernard S. Ab initio molecular dynamics description of proton transfer at water-tricalcium silicate interface. *Cement and Concrete Research* 2020, **136:** 106162.

28. Claverie J, Bernard F, Cordeiro JMM, Kamali-Bernard S. Water's behaviour on Ca-rich tricalcium

silicate surfaces for various degrees of hydration: A molecular dynamics investigation. *Journal of Physics and Chemistry of Solids* 2019, **132:** 48-55.

29. Qi C, Manzano H, Spagnoli D, Chen Q, Fourie A. Initial hydration process of calcium silicates in Portland cement: A comprehensive comparison from molecular dynamics simulations. *Cement and Concrete Research* 2021, **149:** 106576.

30. Réocreux R, Girel É, Clabaut P, Tuel A, Besson M, Chaumonnot A*, et al.* Reactivity of shape-controlled crystals and metadynamics simulations locate the weak spots of alumina in water. *Nature communications* 2019, **10**(1)**:** 1-8.

31. Khachani M, El Hamidi A, Halim M, Arsalane S. Non-isothermal kinetic and thermodynamic studies of the dehydroxylation process of synthetic calcium hydroxide Ca (OH) 2. *J Mater Environ Sci* 2014, **5**(2)**:** 615-624.

32. Sun G, Li Z, Liang R, Weng L-T, Zhang L. Super stretchable hydrogel achieved by non-aggregated spherulites with diameters< 5 nm. *Nature communications* 2016, **7**(1)**:** 1-8.

33. Mumme WG. CRYSTAL-STRUCTURE OF TRICALCIUM SILICATE FROM A PORTLAND-CEMENT CLINKER AND ITS APPLICATION TO QUANTITATIVE XRD ANALYSIS. *Neues Jahrbuch Fur Mineralogie-Monatshefte* 1995(4)**:** 145-160.

34. De Noirfontaine M-N, Dunstetter F, Courtial M, Gasecki G, Signes-Frehel M. Polymorphism of tricalcium silicate, the major compound of Portland cement clinker: 2. Modelling alite for Rietveld analysis, an industrial challenge. *Cement and concrete research* 2006, **36**(1)**:** 54-64.

35. Thissen P, Natzeck C, Giraudo N, Weidler P, Wöll C. Hydration of Concrete: The First Steps. *Chemistry–A European Journal* 2018, **24**(34)**:** 8603-8608.

36. Perdew JP, Burke K, Ernzerhof M. Generalized gradient approximation made simple. *Physical review letters* 1996, **77**(18)**:** 3865.

37. Grimme S, Antony J, Ehrlich S, Krieg H. A consistent and accurate ab initio parametrization of density functional dispersion correction (DFT-D) for the 94 elements H-Pu. *The Journal of chemical physics* 2010, **132**(15)**:** 154104.

38. VandeVondele J, Krack M, Mohamed F, Parrinello M, Chassaing T, Hutter J. Quickstep: Fast and accurate density functional calculations using a mixed Gaussian and plane waves approach. *Computer Physics Communications* 2005, **167**(2)**:** 103-128.

39. Goedecker S, Teter M, Hutter J. Separable dual-space Gaussian pseudopotentials. *Physical Review B* 1996, **54**(3)**:** 1703.

40. Hartwigsen C, Gœdecker S, Hutter J. Relativistic separable dual-space Gaussian pseudopotentials

from H to Rn. *Physical Review B* 1998, **58**(7)**:** 3641.

41. VandeVondele J, Hutter J. Gaussian basis sets for accurate calculations on molecular systems in gas and condensed phases. *The Journal of chemical physics* 2007, **127**(11)**:** 114105.

42. Leung K, Rempe SB. Ab initio rigid water: Effect on water structure, ion hydration, and thermodynamics. *Physical Chemistry Chemical Physics* 2006, **8**(18)**:** 2153-2162.

43. Martyna GJ, Klein ML, Tuckerman M. Nosé–Hoover chains: The canonical ensemble via continuous dynamics. *The Journal of chemical physics* 1992, **97**(4)**:** 2635-2643.

44. Nosé S. A molecular dynamics method for simulations in the canonical ensemble. *Molecular physics* 1984, **52**(2)**:** 255-268.

45. Bonomi M, Parrinello M. Enhanced sampling in the well-tempered ensemble. *Physical review letters* 2010, **104**(19)**:** 190601.

46. Brehm M, Thomas M, Gehrke S, Kirchner B. TRAVIS—A free analyzer for trajectories from molecular simulation. *The Journal of chemical physics* 2020, **152**(16)**:** 164105.

47. Jalilehvand F, Spångberg D, Lindqvist-Reis P, Hermansson K, Persson I, Sandström M. Hydration of the calcium ion. An EXAFS, large-angle X-ray scattering, and molecular dynamics simulation study. *Journal of the American Chemical Society* 2001, **123**(3)**:** 431-441.

48. Zhang W, Li S, Hou D, Geng Y, Zhang S, Yin B*, et al.* Study on unsaturated transport of cement-based silane sol coating materials. *Coatings* 2019, **9**(7)**:** 427.

49. Thomas M, Brehm M, Kirchner B. Voronoi dipole moments for the simulation of bulk phase vibrational spectra. *Physical Chemistry Chemical Physics* 2015, **17**(5)**:** 3207-3213.

50. Wesselsky A, Jensen OM. Synthesis of pure Portland cement phases. *Cement and concrete research* 2009, **39**(11)**:** 973-980.

Supplementary Files

This is a list of supplementary files associated with this preprint. Click to download.

- Supplementaryinformation.docx
- VideoS1.mp4